Experimental characterization of collision avoidance in pedestrian dynamics

Daniel R. Parisi,[1,2,*] Pablo A. Negri,[3,2] and Luciana Bruno[4,2]
[1]*Instituto Tecnológico de Buenos Aires. Lavarden 389, (1437) C. A. de Buenos Aires, Argentina*
[2]*Consejo Nacional de Investigaciones Científicas y Técnicas, Argentina*
[3]*Universidad Argentina de la Empresa, Lima 754 (1073), C. A. de Buenos Aires, Argentina*
[4]*Departamento de Física-IFIBA, Facultad de Ciencias Exactas y Naturales, Universidad de Buenos Aires, Ciudad Universitaria (1428) C. A. de Buenos Aires, Argentina*
(Received 9 April 2016; published 29 August 2016)

In the present paper, the avoidance behavior of pedestrians was characterized by controlled experiments. Several conflict situations were studied considering different flow rates and group sizes in crossing and head-on configurations. Pedestrians were recorded from above, and individual two-dimensional trajectories of their displacement were recovered after image processing. Lateral swaying amplitude and step lengths were measured for free pedestrians, obtaining similar values to the ones reported in the literature. Minimum avoidance distances were computed in two-pedestrian experiments. In the case of one pedestrian dodging an arrested one, the avoidance distance did not depend on the relative orientation of the still pedestrian with respect to the direction of motion of the first. When both pedestrians were moving, the avoidance distance in a perpendicular encounter was longer than the one obtained during a head-on approach. It was found that the mean curvature of the trajectories was linearly anticorrelated with the mean speed. Furthermore, two common avoidance maneuvers, stopping and steering, were defined from the analysis of the acceleration and curvature in single trajectories. Interestingly, it was more probable to observe steering events than stopping ones, also the probability of simultaneous steering and stopping occurrences was negligible. The results obtained in this paper can be used to validate and calibrate pedestrian dynamics models.

DOI: 10.1103/PhysRevE.94.022318

I. INTRODUCTION

The collision avoidance mechanism of biological, synthetic, or virtual agents is a relevant problem in several fields, such as pedestrian dynamics, microscopic simulation of transport systems, moving robots, and animation of characters for video games and motion pictures.

After a first wave of operational-level models of pedestrian dynamics, inspired by pioneering models, such as the "social force model" [1,2] and the "bionics-inspired cellular automaton model" [3], a new generation of pedestrian models, which equip the simulated agents with more sophisticated avoidance mechanisms, has been developed in the past years. For instance, Moussaïd *et al.* [4] presented a model using a "cognitive heuristics" to determine the norm and direction of the desired velocity for each agent dynamically during the evolution of the system. Karamouzas *et al.* [5] proposed a method for collision avoidance by modifying the social force model, basically, by replacing the social force term by a new "evasive" force that tends to avoid future collisions. Also, in the model proposed by Wang *et al.* [6], the social term is removed, and pedestrians can actively avoid collisions using the self-driven force that leads pedestrians to the quickest path to destination in the vision field of the simulated pedestrian.

The development of models of this kind requires specific experimental data in order to calibrate and validate them. Most of the data obtained for pedestrians in laboratory conditions correspond to evacuation and unidirectional flows used to study the flow rate at doors and fundamental diagrams. However, experiments of collision avoidance between pedestrian flows at different densities are less frequent in the literature.

We can mention the work of Bamberger *et al.* [7], who studied the crossing flow of pedestrians at relatively high density. The authors reported the formation of unstable stripes (orthogonal to the sum of the velocity vectors of the two main walking directions) and high flow values compatible with not-crossing configurations. Also, Lian *et al.* [8] performed experiments of four-directional intersecting pedestrian flows in high density regimes studying the density-velocity relationship, lane formation, and the effect of an obstacle in the flow patterns. However, the main results of these investigations are macroscopic and do not provide enough details on the individuals' avoidance maneuvers.

At the other extreme (low density experiments), Paris *et al.* [9] presented results for two pedestrians moving perpendicularly. The authors characterized the pedestrians' interaction by means of the speed and orientation of individual trajectories in order to predict the agents' behavior under a potential collision. This information was used to calibrate their proposed model with reactive navigation.

Another related characteristic of microscopic pedestrian trajectories is the lateral swaying produced by the mechanism of human biped walk. Besides the catastrophic consequence when this behavior resonates with a bridge structure [10], it is also relevant for the design of pedestrian computational models.

The effect of swaying has been observed for unidirectional flows at high densities [11], and it has been considered as one of the factors determining the personal space necessary for pedestrians in order to move forward. For example, Pauls [12] proposed that swaying should be taken into account for designing exit widths. Also, Chraibi *et al.* [13] considered

*dparisi@itba.edu.ar

 ©2016 American Physical Society

this lateral displacement in the "generalized centrifugal force model" for pedestrian dynamics. This model was extended by Krausz and Bauckhage [14] in order to reproduce the swaying patterns observed in high density crowds. Hoogendoorn and Daamen [15] studied unidirectional flows through bottlenecks and found a relationship of the swaying movement with the pedestrian velocity: whereas the swaying was high for low velocities ($\sim$0.4 m/s), it decreased for large ones ($\sim$2 m/s).

The experimental swaying referred to above corresponds to pedestrians walking in the same direction, and it is not related to avoiding maneuvers for which the angular deviations are expected to be larger. In this paper, we characterize both kinds of angular deviation within trajectories: the lateral swaying for almost free pedestrians and the steering maneuvers in order to avoid other pedestrians.

Navigation pedestrian models require more experimental data ranging from low to high density scenarios and considering crossing and head-on potential collisions. Also, new "macroscopic" observables describing avoidance behavior should be defined. These are the objectives of the experiments and analyses performed in the present paper.

II. PEDESTRIAN EXPERIMENTS

The experiments consisted of recording the two-dimensional (2D) trajectories of walking pedestrians and analyzing their avoidance behavior under different conditions.

The experiments were performed with the participation of 20 volunteers (females and males about 22 years old) in an empty parking lot at the Instituto Tecnológico de Buenos Aires. Each volunteer wore a white cap in order to hide their identity and to facilitate subsequent image processing. During the whole experiment, each pedestrian only had to walk less than 500 m (not continuously) inside the measurement area at normal speed and behavior and with no physical contact. Under these conditions, the experimental protocol did not involve any kind of risk, protecting the integrity, privacy, and confidentiality of the personal information of the research subjects.

A GoPro 3 camera was placed in the zenithal position (top-down view) at 4 m height from the floor. It captured the dynamics of the pedestrians within an area of $\sim 5\times \sim 2.8$ m^2 (in the x and y directions, respectively) at $z \sim 1.7$ m, z being the height from the floor. The total image size was 1920×1080 pixels, and the movies were captured at 30 frames/s, so the data obtained were sampled at $\Delta t = 1/30$ s. In order to avoid the transient part of the trajectories near the starting and ending points, the analysis on the x axis was limited to the range of $x \in (-1.6, 1.6$ m). Due to the aspect ratio of the image, it was not necessary to further limit the y axis lying in the range of $y \in (-1.4, 1.4$ m).

Pedestrians were tracked using the center position of the cap to estimate their individual vertical axis, which minimizes the lens deformation. The tracking technique used in this paper allowed assigning a unique label to each pedestrian. The following procedures were implemented to recover single pedestrian trajectories from the movies:

(1) a background model [16] to detect the motion in the frame,

(2) a white hat detector using color and shape (ellipse) in the moving regions in order to obtain the position of the person,

(3) the mean shift [17] algorithm and two color spaces, red, green, and blue and YCbCr to follow each detected pedestrian from the sight until exiting the scene.

The next step consisted of reconstructing each pedestrian trajectory from the 2D position on the image to the three-dimensional real world coordinates. The lens distortion of the camera [Fig. 1 (i)] was corrected using the Santana-Cedrés procedure [18]. To this end, parallel thin ropes were placed equidistantly at $z = 1.7$ m from the floor, i.e., approximately the average height of the volunteers, and a picture was taken with the GoPro 3 camera. Then, using a known pattern and the Toscani-Faugueras algorithm [19], the intrinsic camera parameters $\{(f_x, f_y),(c_x, c_y),(k_1, k_2, p_2, p_2, k_3)\}$ were estimated, (f_x, f_y) being the focal lengths in the x and y directions, (c_x, c_y) being the optical center of the image plane (usually, it is the center of the image), and $(k_1, k_2, p_2, p_2, k_3)$ being the distortion coefficients.

We assume that the moving points, given by the centers of the white caps, evolve on the horizontal fixed plane at $z = 1.7$ m. By using the iterative algorithm POSIT adapted to coplanar points [20] and the known references on the ropes of Fig 1.(i), the pose of the camera is estimated, which allows finding the rotation and translation matrices R and T. It is then possible to associate 2D points moving on the image with the trajectories in the real space given by $(x, y, z = 1.7$ m).

The particular configuration of the setup where the trajectories are parallel to the image plane simplifies the analysis of the model deviation. The error (ϵ) can be estimated for any axis in a similar way: We look at the error on the x axis since it is larger than that of the y axis because of the image format. It can be approximated analytically by $\epsilon_x = dh|u - c_x|/f_x$, where dh is the difference in height from the mean value, u is the position of the point on the image, c_x is the center of the image, and f_x is the focal length on this axis. This error increases linearly from zero at the center of the image to a maximum at the boundaries of the region of interest. Considering that 95% of the participants are between 1.61 and 1.79 m tall, then $dh = 9$ cm. Having $f_x = 1884$ pixels and $c_x = 957$, the maximum error on the x axis at the boundaries of the region of interest ($u = 1708$ pixels) is $\max(\epsilon_x) = 3.58$ cm.

Several configurations of potential collisions between pedestrians were studied. To this end, the participants were divided into two groups, and each group was asked to walk in a certain direction. The direction of movement was along the x axis or x and y axes in order to study head-on or crossing at 90° encounters for different flows and group sizes, respectively. All the configurations considered in this study are shown in Fig. 1.

We will refer to these data as the raw coordinates of the trajectory $\mathbf{r}_r(t) = [x_r(t), y_r(t)]$. Because the tracking algorithm has a finite precision in the determination of the pedestrian position, high frequency fluctuations can be present in these raw trajectories. Examples of raw trajectories are shown as circles in Fig. 2(a). Thus, we further smooth each trajectory by fitting a generalized regression neural network (GRNN) from

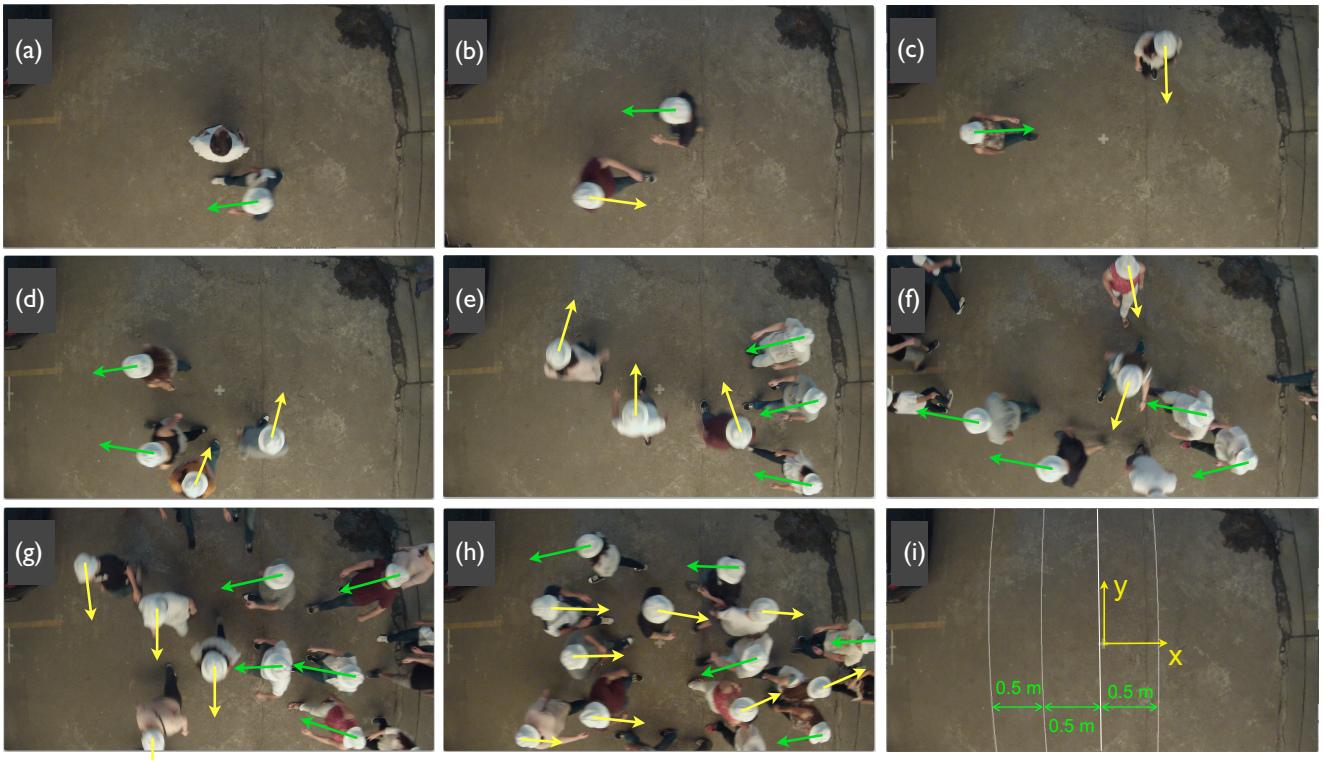

FIG. 1. Snapshots of avoidance experiments. The arrows indicate the pedestrians' direction of motion. (a) One pedestrian avoiding another arrested pedestrian, which can be considered as an elliptical obstacle. (b) One to one head-on pedestrian avoidance. (c) One to one perpendicular crossing. (d) and (e) Two groups of two (d) and three (e) pedestrians in a perpendicularly crossing situation. (f) Two lines of pedestrians in a perpendicular crossing. The average flow of each line is 0.9 pedestrian/s. (g) and (h) Two groups of ten pedestrians in a perpendicular crossing (g) and in a counterflow configuration (h). (i) Parallel white ropes separated by 0.5 m, placed at 1.7 m from the floor for correcting lens deformation and calibrating distance units.

the MATLAB NN toolbox [21] to each coordinate as a function of time $\mathbf{r}_r(t) \sim \mathbf{r}(t) = [x(t), y(t)]$, where $x(t)$ and $y(t)$ are the GRNN fittings of $x_r(t)$ and $y_r(t)$, respectively. This kind of network has a radial (Gaussian) basis function layer and has the advantage of having only one parameter: the spread (sp). In our case, we use $\mathrm{sp} = 3\,\Delta t = 0.1$ s, producing the desired smoothed trajectories. This allows us to calculate speeds and curvatures by the discrete derivation of $\mathbf{r}(t)$ using the highest sampling frequency given by the camera (30 fps). Examples of the GRNN fitting can be seen as solid line curves in Fig. 2(a) (which are placed over the raw trajectories plotted as circles). From now on, only the smoothed trajectories $\mathbf{r}(t)$ will be used in the analysis.

III. RESULTS

A. Free pedestrians

First, we characterized the almost free trajectories in experiments where only two pedestrians are present. These configurations are shown in Figs. 1(a)–1(c).

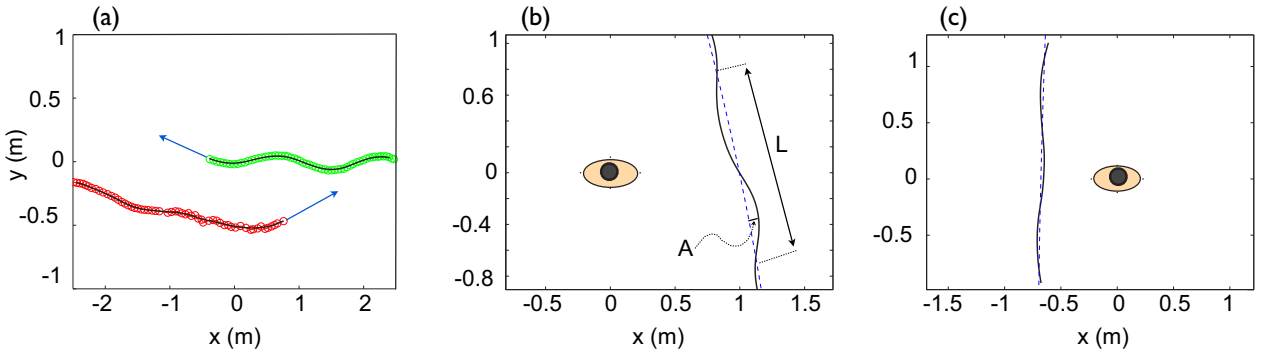

FIG. 2. Recovered trajectories. (a) Two representative recovered trajectories (circles) and their NN fitting $\mathbf{r}$ (solid line). (b) Lateral swaying: definition of the amplitude (A) and period (L). The solid line corresponds to the smoothed trajectory $\mathbf{r}$, and the dashed one represents the main direction of motion determined using the quadratic fitting ($\mathbf{r}'$). The ellipse at $(x, y) = (0,0)$ represents an arrested pedestrian. (c) Another trajectory displaying less lateral swaying (lower A).

1. Amplitude and period of swaying

As already mentioned, pedestrians display a lateral swaying related to the mechanism of biped motion. In order to quantify this oscillation we first determined the main direction of motion. To this end, we computed the quadratic fitting of each component of the smooth trajectory ($\mathbf{r}$), i.e., $x(t)$ and $y(t)$ as functions of time. The resulting trajectory, $\mathbf{r}' = [x'(t), y'(t)]$ [where $x'(t) = px_2t^2 + px_1t + px_0$ and $y'(t) = py_2t^2 + py_1t + py_0$ are the fitted data, px_i and py_i being the coefficient found by least squares], represents the main direction of motion. Examples of the quadratic fitting of smoothed trajectories can be seen in Figs. 2(b) and 2(c) as dashed lines. Then, the amplitude (A) and period (L) of the lateral swaying were obtained as the maximum distance from the trajectory $\mathbf{r}$ to its quadratic fitting $\mathbf{r}'$ and the segment between three successive crossings of $\mathbf{r}$ and $\mathbf{r}'$, respectively [Fig. 2(b)].

It should be noted that the fitted trajectories $\mathbf{r}'$ are only used in the present subsection considering the free-pedestrian scenarios given by the 20 trajectories of a single pedestrian walking along the x or y direction in the presence of an arrested one [see Fig. 1(a)]. Both directions of motion provide data compatible with the same distribution of parameter values. The obtained period was $L = 1.60 \pm 0.28$ m (mean $\pm$ standard deviation), whereas the amplitude took a value of $A = 0.036 \pm 0.024$ m. We assume these values as the ones corresponding to the free walking of a single pedestrian's experimental condition.

The obtained swaying amplitude is in agreement with the one reported in Ref. [15] ($\sim$0.04 m) for the range of pedestrian velocities (1.4–1.7 m/s). This range corresponds to the one measured in our experiments [see Fig. 6(a)].

2. Minimum avoidance distance

In order to characterize avoidance events between pairs of pedestrians, we computed the distance between two subjects considering their smoothed trajectories $\mathbf{r}_i$ and $\mathbf{r}_j$ in every frame as $d(t) = \{[x_i(t) - x_j(t)]^2 + [y_i(t) - y_j(t)]^2\}^{1/2}$ and defined the minimum avoidance distance $d_{\min}$ when $d(t)$ is minimum. In the case of one moving pedestrian and an arrested one [Fig. 1(a)], we evaluated $d_{\min}$ for pedestrians moving in the x and y directions. Considering that the stalled pedestrian has an approximately elliptical shape with its large axes orientated in the x-axis direction, walking in the x and y directions is not a symmetrical condition due to the different "impact section" seen by the walking pedestrian. However, we found that $d_{\min}$ did not depend on the direction of the path (Table I). On the other hand, two converging pedestrians in perpendicularly crossing trajectories, such as the one shown in Fig. 1(c), displayed larger values of $d_{\min}$ than those found during head-on encounters [Fig. 1(b)]. Table I displays the mean and standard deviations of $d_{\min}$ obtained for these four configurations.

3. Instantaneous speed

The pedestrians' instantaneous speed was computed from the trajectories $\mathbf{r}$ as $v(t) = \frac{\Delta r}{\Delta t}$, where $\Delta r = (\Delta x^2 + \Delta y^2)^{1/2}$ and $\Delta t = 1/30$ s, the camera sampling time. The spatial difference (Δr) is calculated as the difference between the current position and the position in the previous frame.

TABLE I. Minimum avoidance distance for two-pedestrian experiments. The first two lines correspond to the same distribution and thus can be considered equal. The last two differ significantly (Kolmogorov-Smirnov test: p value < 0.0015).

Configuration	$\langle d_{\min} \rangle$ (m)	$\sigma(d_{\min})$ (m)
Figure 1(a), y direction	0.77	0.12
Figure 1(a), x direction	0.73	0.12
Figure 1(b) (head-on)	0.71	0.13
Figure 1(c) (perpendicular)	1.00	0.18

Figure 3 shows the distribution of instantaneous speeds obtained in the two-pedestrian experiments [Figs. 1(a)–1(c)]. In total, 74 trajectories were analyzed. The speeds displayed a normal distribution behavior with a mean value equal to 1.66 and $\sigma = 0.24$ m/s. Furthermore, no differences were found between the mean speeds before and after the avoidance event.

B. Collective avoidance behavior

We investigate here the steering and navigation maneuvers performed by pedestrians to avoid collisions between them. To this end, we will consider the following three quantities derived from the trajectories: (a) the instantaneous speed v as defined above; (b) the magnitude of the instantaneous acceleration computed as $a = \frac{\Delta v}{\Delta t}$; and (c) the instantaneous angular change in the velocity direction defined as $\omega = \frac{\theta}{\Delta t}$, where θ is the positive minimum angle between two consecutive vectors $\mathbf{dr} = [\mathbf{r}(t) - \mathbf{r}(t - \Delta t)]$. The determination of θ involves three consecutive points in the trajectory as shown in Fig. 4.

The change in direction $\omega(t)$ is a measure of the curvature of the trajectory. Because of the lateral swaying, an oscillatory behavior of $\omega(t)$ is expected. Also, the magnitudes of the acceleration $a(t)$ and the speed $v(t)$ display this kind of behavior (Fig. 5).

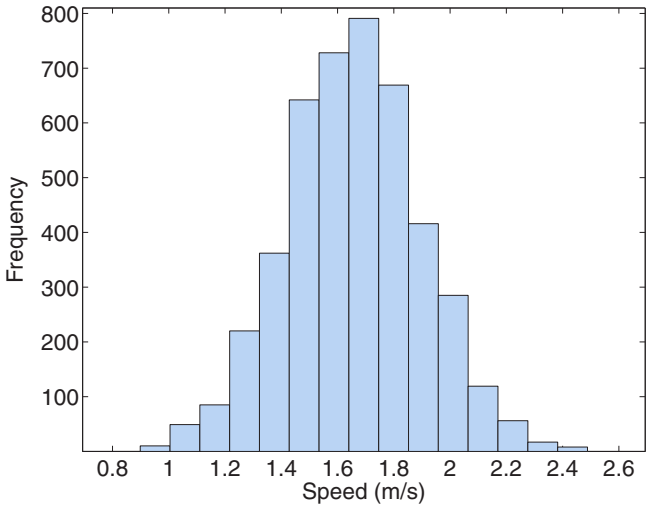

FIG. 3. Instantaneous speeds of two-pedestrian experiments. Histogram obtained from 74 trajectories corresponding to the configurations shown in Figs. 1(a)– 1(c). The mean value is $\langle v \rangle = 1.66$ m/s, and the standard deviation is $\sigma = 0.24$ m/s.

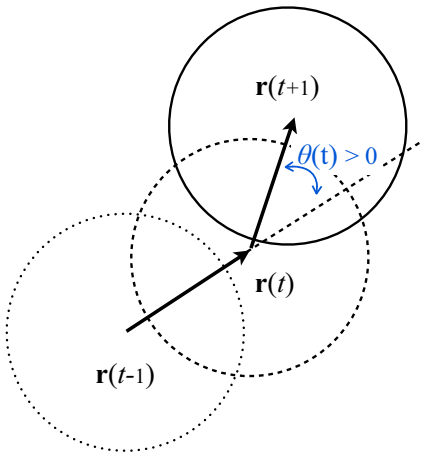

FIG. 4. Definition of angle $\theta(t)$ to characterize the curvature of trajectories.

In order to build an overall picture of pedestrians' avoidance maneuvers, we studied the behavior of these three magnitudes in the configurations shown in Fig. 1. We estimated the mean values and standard deviations of ω, v, and a averaging over time and trajectories and analyzed their mutual dependence.

In Fig. 6(a) we plot the average angular change rate ($\langle\omega\rangle$) against the average instantaneous speed ($\langle v\rangle$). A clear trend can be observed, indicating that, as the mean speed decreases (corresponding to an increase in the number of pedestrians), the mean curvature $\langle\omega\rangle$ increases. This behavior can be understood if we consider that pedestrians act as obstacles or barriers between them that need to be avoided and, therefore, when the density is large, the pedestrian trajectories display greater changes in direction.

In order to quantify the variations within each trajectory in terms of directionality and speed changes we computed the maximum angular change and the speed dispersion in

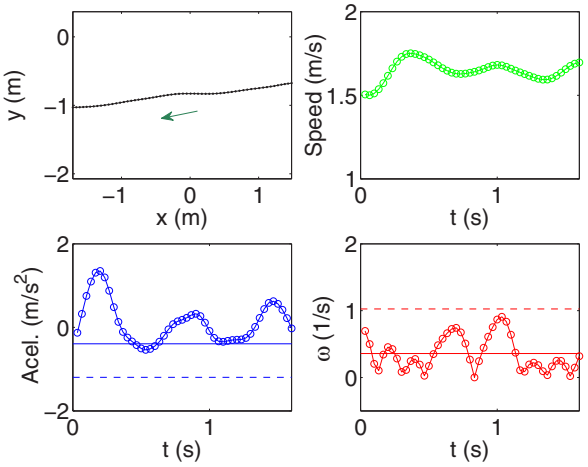

FIG. 5. Key variables derived from one representative trajectory of a free pedestrian. The upper left panel depicts the trajectory, and the arrow indicates the forward direction; the upper right panel shows the speed evolution, and the lower panels display the acceleration and curvature, respectively. The solid and dashed lines represent the mean and threshold values that are explained below (see Fig. 7).

every single trajectory. The latter was defined as $[\max(v) - \min(v)]/\langle v\rangle$. In Fig. 6(b) we show these two quantities averaged over all trajectories from each data set. The linear correlation found indicates that, when the number of pedestrians and hence the complexity of the avoidance increases, both the speed dispersion and the directionality spread also increase.

However, since the data shown in Fig. 6 are average values, it is not possible to distinguish whether both effects, i.e., large changes in speed and directionality, occur within the same trajectory and/or simultaneously. In order to assess this question, we focused on two main avoidance maneuvers: abrupt change in direction (steering) and abrupt speed reduction (stopping).

To recognize these particular events (e), we used a threshold criterion. A steering event occurs when $\omega(t)$ exceeds a threshold value given by $\omega_{\text{thr}} = 2.8 \times \sigma(\omega)$, where σ is the standard deviation of $\omega(t)$ in each trajectory. Similarly, a stopping event is defined only for negative accelerations when $a(t)$ decreases below a_{thr} with $a_{\text{thr}} = -2.8 \times \sigma(a^-)$, considering the standard deviation of a^-, i.e., computed for the set of values of a fulfilling the condition $a < 0$. Examples of only steering, only stopping, and steering and stopping events are shown in Figs. 7(a)–7(c), respectively. Each pair of panels in Fig. 7 displays $a(t)$ and $\omega(t)$, corresponding to the same trajectory. Typically, avoidance maneuvers occur independently of one another [Figs. 7(a) and 7(b)]. However, both events can occur simultaneously [Fig. 7(c)]. In this case, we assumed that both maneuvers are correlated when the separation in time between the events is less than $3\,\Delta t$ ($= 3/30$ s $= 0.1$ s).

Furthermore, we also defined the start time (t_0) of an abrupt avoidance maneuver as the data point just before crossing the mean value. Thus, the anticipation time (t_e) of a given maneuver is the time elapsed since t_0 up to the first data point of the avoidance event. In Fig. 7, these data points are signaled with arrows.

Looking only at the abrupt avoidance maneuvers defined above (events e), the anticipation time is independent of the density and velocity, showing a uniform value of $t_e = 0.15 \pm 0.04$ s for steering events and, very close to it, $t_e = 0.13 \pm 0.02$ s for stopping ones. And the mean values of angular velocity and deceleration are $\langle\omega_e\rangle = 2.3\ \text{s}^{-1}$ and $\langle a_e\rangle = -2.5\ \text{ms}^{-2}$, respectively. These quantities are listed in Table II.

We then studied the frequency of occurrence of the different avoidance maneuvers. The probability of occurrence of an event (e) being steering, stopping, or both simultaneously was estimated as $P_e = \frac{N_e}{N}$, where N_e is the number of trajectories having positive events and N is the total number of trajectories in the set. We selected 290 trajectories having at least 50 data points ($\sim$1.67 s) after skipping the first and the last 20% in order to avoid border artifacts as explained in Sec. II. For each trajectory set corresponding to the configurations shown in Fig. 1, we computed the probability of occurrence of the different events. The results are shown in Fig. 8.

Many interesting features can be derived from Fig. 8. For the low density configurations, corresponding to head-on and crossing trajectories of few (up to four) simultaneous pedestrians [Figs. 1(a)–1(d)], stopping events are not observed. Under space availability conditions, the only avoidance maneuver

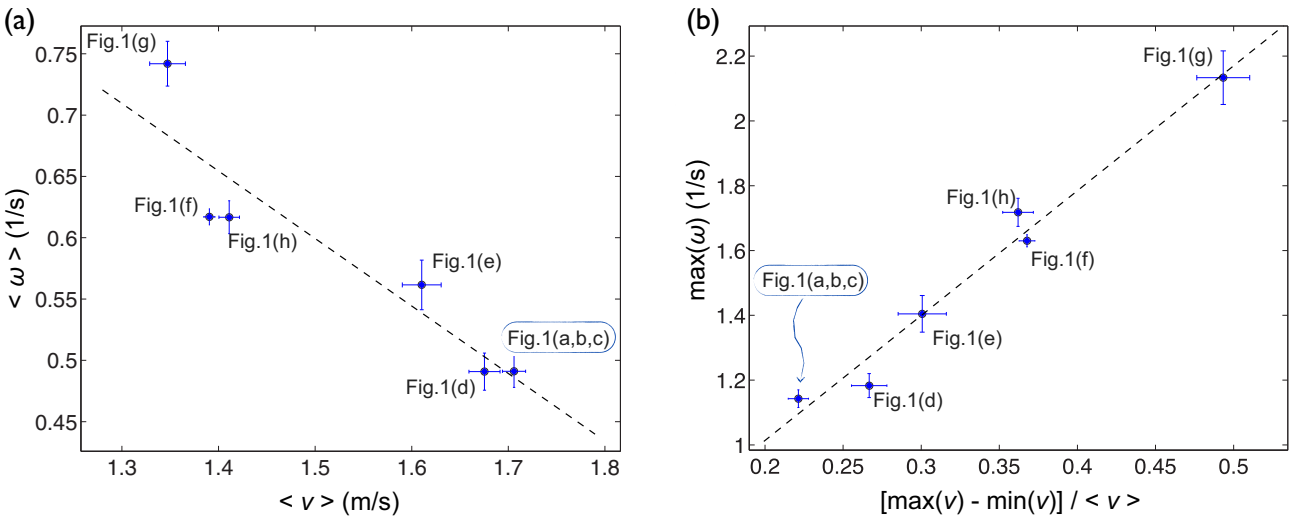

FIG. 6. Relationship between curvature and speed for pedestrian trajectories. Each symbol represents the average and standard deviation for all trajectories corresponding to each experimental configuration shown in Fig. 1. (a) Angular change rate versus speed. (b) Maximum angular change rate for each trajectory versus the difference between extreme values of the velocity normalized by its mean value.

observed is steering without abrupt deceleration. When the number of pedestrians increases, the stopping and steering frequencies also increase. It must be noted that experiment II–V [configurations illustrated in Figs. 1(d)–1(g)] correspond to perpendicularly crossing trajectories.

On the other hand, experiment VI [Fig. 1(h)] is a potential head-on collision experiment, and for this case, the probability of steering slightly decreases with respect to the one obtained in experiment V for the same group size but in a crossing configuration [Fig. 1(g)]. On the contrary, the stopping probability in experiment VI is larger than that corresponding to the perpendicularly crossing case, i.e., experiment V. This suggests that head-on encounters may need less pronounced steering events, which is consistent with the lower minimum distance needed in the same case for almost free pedestrians, as seen in Sec. III A 2.

To summarize, the global probabilities of avoidance events considering all 290 trajectories were $P_{\text{steering}} = 0.31$, $P_{\text{stopping}} = 0.10$, and $P_{\text{steering-and-stopping}} = 0.02$. The coexistence of both avoidance events (steering and stopping simultaneously) was very low in every experiment, suggesting that pedestrians choose between one maneuver (e.g., steering) at the expense of the other (e.g., stopping).

We then wondered whether simultaneous events of this kind can be considered a third avoidance behavior or they are just a coincidence in time of the other two maneuvers. In order to explore the frequency of the occurrence of steering-and-stopping events, each trajectory was divided into M segments of duration $3\,\Delta t$, i.e., corresponding to the time window chosen to resolve separate events. Then, the overall probability of steering per segment was computed as $p_{\text{steering}} = \frac{n_s}{NM}$, where n_s is the number of positive steering events and N is the total number of trajectories. In the same way, we determined the probabilities of stopping, and steering-and-stopping per segment. We obtained $p_{\text{steering}} = 0.019$, $p_{\text{stopping}} = 0.006$, and $p_{\text{steering-and-stopping}} = 0.0015$. Interestingly, the conditional probability of steering and stopping simultaneously, considered as independent random variables, is as follows: $p_{\text{steering}} \times p_{\text{stopping}} = 0.0001$. This value is more than an order of magnitude lower than the one determined in the experiments, suggesting that the combined maneuver, although rare, can be considered a third kind of maneuver.

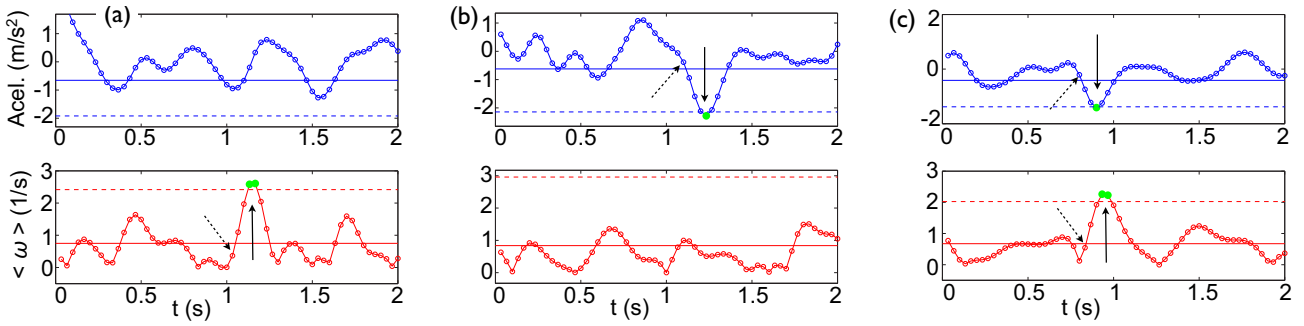

FIG. 7. Time evolution of acceleration and angular velocity for three trajectories. In all cases, the solid line represents the mean value, and the dashed line is the threshold value of $2.8 \times \sigma$ as explained in the text. (a) One steering event and no stopping one. (b) Stopping event but not a steering one. (c) Stopping and steering events occurring simultaneously. Vertical arrows indicate events, i.e., values beyond thresholds. The dashed and tilted arrows indicate the start of the maneuver.

TABLE II. Values of angular velocity, deceleration, and anticipation time for both kinds of avoidance events.

Avoidance event (e)	Mean	Variance
ω_e	2.3 s^{-1}	1.6 s^{-1}
a_e	-2.5 ms^{-2}	0.9 ms^{-2}
$t_e(\omega_e)$	0.15 s	0.04 s
$t_e(a_e)$	0.13 s	0.02 s

IV. CONCLUSIONS

In this paper, we experimentally investigated some features of pedestrians' avoidance mechanisms in crossing and head-on encounters for different flow rates and group sizes. To this end, we recorded, with high time resolution, the motion of pedestrians walking in predefined ways. The 2D trajectories were recovered from the movies and analyzed.

In the case of very low pedestrian densities, the swaying amplitude (A) and length of one walking cycle, i.e., two consecutive steps L were measured, obtaining $A = 0.036 \pm 0.024$ and $L = 1.60 \pm 0.28$ m. Also, the minimum distances of encounter between two subjects were determined. We found that, when one pedestrian is arrested and not moving, the minimum distance ($d_{\min} \sim 0.75$ m) is independent of the direction of the walking pedestrian with respect to the torso orientation of the arrested one. On the other hand, when both pedestrians are moving, the minimum avoidance distance is greater ($d_{\min} \sim 1$ m) in the case of a potential perpendicular collision than in the case of a head-on conflict situation ($d_{\min} \sim 0.68$ m).

We also studied the maneuver mechanisms for different pedestrian densities. We proposed a criterion for defining abrupt avoidance events (stopping and steering) from the analysis of acceleration and curvature of single trajectories. Our results showed that the frequency of both evasive maneuvers increases with the number of pedestrians. Also, it is about three times more probable to avoid another pedestrian by changing the direction of motion (steering) than by an abrupt deceleration (stopping). In other words, if there is enough available space, pedestrians prefer to change their direction of movement rather than decrease their speed.

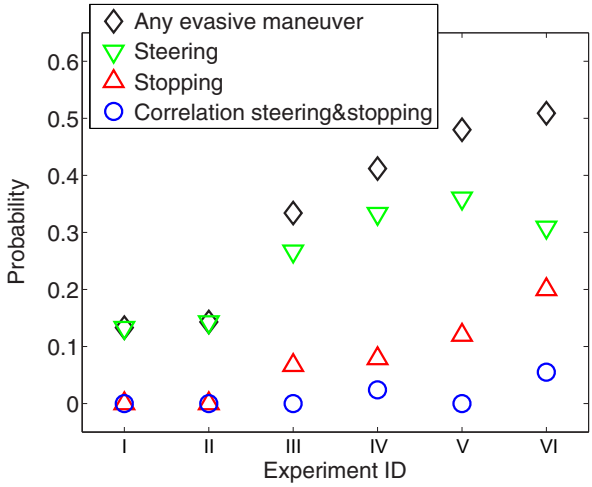

FIG. 8. Approximate probabilities of having avoidance events for the different configurations studied. (I) Experiments described in Figs. 1(a)–1(c), (II) Fig. 1(d), (III) Fig. 1(e), (IV) Fig. 1(f), (V) Fig. 1(g), and (VI) Fig. 1(h). The configurations are ordered by increasing the number of total events (rhombus).

Finally, we found that the probability of steering-and-stopping per trajectory is very low ($P_{\text{steering-and-stopping}} = 0.02$). However, a detailed analysis of the probabilities of occurrence of these simultaneous events showed that they can be considered as a new type of maneuver different from steering and stopping.

We expect that the data obtained from these pedestrian avoidance experiments and their subsequent analysis will be useful to validate and calibrate models in the area of pedestrian dynamics simulation.

ACKNOWLEDGMENTS

This work was funded by Grant PICT-2011 No. 1238 (Agencia Nacional de Promoción Científica y Tecnológica, Argentina), Grant ACyT No. A15T14 (UADE, Argentina), and Grant ITBACyT-2015 No. 33 (ITBA, Argentina). The authors also want to thank all the volunteers participating in the experiments and Professor P. G. König for inviting them.

[1] D. Helbing and P. Molnar, Social force model for pedestrian dynamics, Phys. Rev. E **51**, 4282 (1995).

[2] D. Helbing, I. J. Farkas, and T. Vicsek, Simulating dynamical features of escape panic, Nature (London) **407**, 487 (2000).

[3] A. Kirchner and A. Schadschneider, Simulation of evacuation processes using a bionics-inspired cellular automaton model for pedestrian dynamics, Physica A **312**, 260 (2002).

[4] M. Moussaïd, D. Helbing, and G. Theraulaz, How simple rules determine pedestrian behavior and crowd disasters, Proc. Natl. Acad. Sci. USA **108**, 6884 (2011).

[5] I. Karamouzas, P. Heil, P. van Beek, and M. H. Overmars, A Predictive Collision Avoidance Model for Pedestrian Simulation, *Motion in Games* (Springer, Berlin/Heidelberg, 2009), pp. 41–52.

[6] Q.-L. Wang, Y. Chen, H.-R. Dong, M. Zhou, and B. Ning, A new collision avoidance model for pedestrian dynamics, Chin. Phys. B **24**, 038901 (2015).

[7] J. Bamberger, A. L. Geßler, P. Heitzelmann, S. Korn, R. Kahlmeyer, X. H. Lu, Q. H. Sang, Z. J. Wang, G. Z. Yuan, M. Gauß, and T. Kretz, Crowd Research at School: Crossing Flows, *Traffic and Granular Flow '13* (Springer, Cham, Switzerland, 2015), pp. 137–144.

[8] L. Lian, X. Mai, W. Song, Y. K. K. Richard, X. Wei, and J. Ma, An experimental study on four-directional intersecting pedestrian flows, J. Stat. Mech.: Theory Exp. (2015) P08024.

[9] S. Paris, J. Pettr, and S. Donikian, Pedestrian reactive navigation for crowd simulation: a predictive approach, Comput. Graph. Forum **26**, 665 (2007).

[10] E. T. Ingólfsson, C. T. Georgakis, and J. Jönsson, Pedestrian-induced lateral vibrations of footbridges: A literature review, Eng. Struct. **45**, 21 (2012).

[11] J. J. Fruin, *Pedestrian Planning and Design*, edited by University of Michigan (Metropolitan Association of Urban Designers and Environmental Planners, Michigan, USA, 1971).

[12] J. L. Pauls, Stairways and ergonomics, *ASSE Professional Development Conference and Exposition* (American Society of Safety Engineers, Seattle, 2006), pp. 11–14.

[13] M. Chraibi, A. Seyfried, and A. Schadschneider, Generalized centrifugal-force model for pedestrian dynamics, Phys. Rev. E **82**, 046111 (2010).

[14] B. Krausz and C. Bauckhage, Integrating Lateral Swaying of Pedestrians into Simulations, *Pedestrian and Evacuation Dynamics 2012* (Springer, Cham, 2014), pp. 729–737.

[15] S. P. Hoogendoorn and W. Daamen, Pedestrian behavior at bottlenecks, Transportation Science **39**, 147 (2005).

[16] P. KadewTraKuPong and R. Bowden, An improved adaptive background mixture model for real-time tracking with shadow detection, *Video-Based Surveillance Systems, Computer Vision and Distributed Processing* (Springer, Berlin, 2001), pp. 135–144.

[17] D. Comaniciu, V. Ramesh, and P. Meer, Real-time tracking of non-rigid objects using mean shift, in *IEEE Conference on Computer Vision and Pattern Recognition, Hilton Head, SC, 2000*, (IEEE, Piscataway, NJ, 2000), Vol. 2, pp. 142–149.

[18] D. Santana-Cedrés, L. Gomez, M. Aleman-Flores, A. Salgado, J. Esclarín, L. Mazorra, and L. Alvarez, Invertibility and estimation of two-parameter polynomial and division lens distortion models, SIAM J. Imaging Sci. **8**, 1574 (2015).

[19] R. Horaud and O. Monga, *Vision par Ordinateur: Outils Fondamentaux*, 2nd ed. (Hermes, New Castle, PA, 1995).

[20] D. Oberkampf, D. F. DeMenthon, and L. S. Davis, Iterative Pose Estimation Using Coplanar Feature Points, Comput. Vis. Image Underst. **63**, 495 (1996).

[21] P. D. Wasserman, *Advanced Methods in Neural Computing* (Van Nostrand-Reinhold, New York, 1993).